Theoretical and Applied Fracture Mechanics 122 (2022) 103647

Contents lists available at ScienceDirect

Theoretical and Applied Fracture Mechanics

journal homepage: www.elsevier.com/locate/tafmec

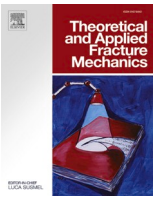

Buckling-induced delamination: Connection between mode-mixity and Dundurs parameters

S. Zak [a,*], A. Lassnig [a], M. Hrstka [b], M.J. Cordill [a,c]

[a] Erich Schmid Institute of Materials Science, Austrian Academy of Sciences, Jahnstraße 12, Leoben 8700, Austria
[b] Institute of Solid Mechanics, Mechatronics and Biomechanics, Faculty of Mechanical Engineering, Brno University of Technology, Technická 2896/2, Brno 616 69, Czech Republic
[c] Department of Materials Science, Chair of Material Physics, Montanuniversität Leoben, Jahnstraße 12, Leoben 8700, Austria

ARTICLE INFO

Keywords:
Delamination fracture
Elastic properties
Finite element modelling
Mixed-mode I+II
Thin film

ABSTRACT

Modern electronics, micromechanical devices and applications demanding high reliability to weight or cost ratio consist of various combinations of multilayered thin films on rigid and compliant substrates, whereas the used materials can differ in their mechanical properties. In recent years, differences in the elastic moduli and Poisson's ratios of such structures are becoming more pronounced. Therefore, a strong push to investigate interface stability with a more in-depth view on the elastic material properties mismatch influence is needed. Measurements of the adhesion of thin films on different substrate materials can be easily performed by the spontaneous buckling method described by Hutchinson and Suo. However, the original approach assumes several simplifications. One is to omit the changes of the influence of the elastic mismatch between the thin film and substrate on the basis of small variations in then-used materials, which is not true for modern materials combinations with vastly different elastic properties. The elastic mismatch on the interface between two different materials can be described by the Dundurs parameters. In this work, finite element modelling is combined with analytical solutions according to general description of the original model to extend the usability of the Hutchinson and Suo method for use with more different materials with higher accuracy. Obtained results point out the fact that disregarding the Dundurs parameters introduces significant errors in evaluating adhesion energy in relation to loading mode, proving the necessity to properly include elastic mismatch.

1. Introduction

In recent years, there were significant advances in the wearable and flexible electronics industry for applications in medicine and biomechanics [1–6], electronic devices [7–12] and protective coatings [13–17] in terms of the use of the thin films and coatings. One common factor of the somewhat different fields of applications is the use of a wide range of materials and their diversity in terms of the elastic material properties. To achieve a satisfactory function and reliability of the device made out of modern materials, there is a high demand on material engineering. In a flexible component, such as a bio-sensor plate or bendable display, there is always a combination of a compliant substrate material and a metallic or ceramic thin film, usually stacked in numerous layers. The protective coating applications demand the use of hard, rigid thin layers on more ductile or brittle substrates. Even though the used materials can be engineered to have high strength and reliability with dimensions on the micro- and nano-scale, there is still a need to ensure a strong bond between the film and substrate, where the interface between the film and substrate is considered to be a "weak link". The interface susceptibility to damage may be even more pronounced when strongly dissimilar materials are used in combination with various loading regimens and/or harsh environmental conditions (large strains, temperature changes, etc.). Therefore, a special effort to investigate the strength and reliability of thin film – substrate interfaces is needed. Moreover, the mentioned modern applications bring more attention to the material property mismatch, which can be described by

Abbreviations: BF-STEM, Bright field scanning transmission electron microscopy; BPSG, Boro-phosphor-silicate glass; CLSM, Confocal laser scanning microscopy; FE, Finite element; FIB, Focused ion beam; FQ, Fused quartz; H&S, Hutchinson and Suo; HEA, High entropy alloy; PI, Polyimide; SIFs, Stress intensity factors; TF-MG, Thin film metallic glass.

* Corresponding author at: Jahnstraβe 12, 8700 Leoben, Austria.
E-mail address: stanislav.zak@oeaw.ac.at (S. Zak).

https://doi.org/10.1016/j.tafmec.2022.103647
Received 20 September 2022; Received in revised form 19 October 2022; Accepted 19 October 2022
Available online 31 October 2022

the Dundurs parameters [18,19]. It is important to note that Dundurs parameters α and β have been the backbone of thin film fracture mechanics, but are generally rooted in metal/ceramic interfaces [20–24] rather than metal/polymer or ceramic/polymer interfaces. The Dundurs parameters are defined by the thin film and substrate shear moduli μ_1 and μ_2 and their Poisson's ratios ν_1 and ν_2, respectively:

$$\alpha = \frac{\mu_1(1-\nu_2)-\mu_2(1-\nu_1)}{\mu_1(1-\nu_2)-\mu_2(1-\nu_1)},$$
$$\beta = \frac{1}{2}\frac{\mu_1(1-2\nu_2)-\mu_2(1-2\nu_1)}{\mu_1(1-2\nu_2)+\mu_2(1-2\nu_1)}. \quad (1)$$

Different methods for measuring thin film adhesion energy can be used. A buckling delamination can be initiated by controlled indentation [20,25,26], requiring rigid substrate, tensile-induced buckling [27–29], requiring compliant substrate or by a straightforward method called the spontaneous buckling-delamination by Hutchinson and Suo (H&S) [20], exploiting the spontaneous buckling delamination due to high compressive stresses in the film, whereas its usability was demonstrated for different film-substrate systems (see e.g. [25,30–32]). The model is based on Euler's solution of the elastic beam [33] applied on the one-sided blister of the thin film formed due to the compressive residual stress stored in the film.

The compressive stress in the thin film can be either specifically tailored for the purposes of the adhesion measurement by control over the deposition parameters, through the addition of a stressed overlayer [32], thermal loading [31] or as a by-product of the thin layer fabrication (e.g. thermal expansion coefficients mismatch or side effects of the specialized method used for film deposition [34–38]). While the techniques to introduce the residual stress in the thin film are of interest, it is not the focus of this work. Therefore, let's assume the existence of the stress σ in the film causing its delamination and forming a straight buckle (as depicted in Fig. 1 b) where the buckle cross-section can be modelled as a 2D blister according to Fig. 1 a. Measurements of the film thickness h, buckle height δ and buckle half-width b together with the thin film Young's modulus E_1 and Poisson's ratio ν_1 can be then used in H&S model [20] to evaluate the adhesion energy $\Gamma(\Psi)$ for the plane strain case:

$$\Gamma(\Psi) = \frac{(1-\nu_1^2)h}{2E_1}(\sigma-\sigma_c)\cdot(\sigma+3\sigma_c) \quad (2)$$

where σ_c denotes the critical buckling stress and for the case of plane strain it is defined as [20,39]:

$$\sigma_c = \frac{\pi^2}{12}\frac{E_1}{(1-\nu_1^2)}\left(\frac{h}{b}\right)^2 \quad (3)$$

The variable Ψ is the mode-mixity parameter denoting the mode II to mode I stress intensity factors (SIFs) K_{II} to K_I ratio and can be evaluated from the buckle height to width ratio $\xi = \delta/h$ and the phase factor ω [20], or from the initial stress in the thin film σ, the critical buckling stress σ_c and the phase factor ω [20,39]:

$$\tan(\Psi) = \frac{K_{II}}{K_I} = \frac{4\cos(\omega)+\sqrt{3}\xi\sin(\omega)}{-4\sin(\omega)+\sqrt{3}\xi\cos(\omega)} = \frac{\cos(\omega)+\frac{1}{2}\left(\sqrt{\frac{\sigma}{\sigma_c}-1}\right)\sin(\omega)}{-\sin(\omega)+\frac{1}{2}\left(\sqrt{\frac{\sigma}{\sigma_c}-1}\right)\cos(\omega)} \quad (4)$$

Both solutions in (4) are equivalent and the use of a specific one depends on the known parameters. The first approach with $\xi = \delta/h$ relates to the geometry of the buckle and approach using σ_c relates to a moment-force balance of the system.

Model from Fig. 1a with solution through eqs. (2) - (4) assumes clamped boundary conditions on the sides of the model. However, for values of $|\alpha|$ above 0.5, the real deformation mismatch between film and substrate causes a deviation from the modelled assumptions. More recent works [40,41] present extensions to critical buckling stress and SIFs with additional terms accounting for the substrate compliance, leading to an explicit expression of the extended critical buckling stress σ_c^* as a function of the buckle geometry, simplified critical buckling stress σ_c from eq. (3) and auxiliary parameters a_{11}, a_{12} and a_{22}:

$$\frac{12b}{\pi h}\sqrt{\frac{\sigma_c}{\sigma_c^*}}\tan\left(\pi\sqrt{\frac{\sigma_c^*}{\sigma_c}}\right)+a_{22}-\frac{a_{12}^2}{1+a_{11}}=0 \quad (5)$$

The auxiliary parameters a_{11}, a_{12} and a_{22} describe non-linear deformation of the buckle and they are defined by the tangential force F and bending momentum M in relation to the displacement u and rotation θ of the buckle at the delamination crack tip position according to coordinate system in Fig. 1a [40]:

$$u(x=b) = a_{11}\frac{F\cdot(1-\nu_1^2)}{E_1}+a_{12}\frac{M\cdot(1-\nu_1^2)}{E_1 h},$$
$$\theta(x=b) = a_{12}\frac{F\cdot(1-\nu_1^2)}{E_1 h}+a_{22}\frac{M\cdot(1-\nu_1^2)}{E_1 h^2}. \quad (6)$$

Parameters a_{11}, a_{12} and a_{22} can be evaluated by solving integral equations of the whole system deformation or with the use of numeric evaluation [40,42,43]. This extended approach allows for a more reliable evaluation of the conditions at the buckle-delamination crack tip for case of $|\alpha| > 0.5$ and $\beta = 0$. However, if cases with $\beta \neq 0$ need to be quantified, a complex value of SIFs has to be used Ψ [20,39,44], leading to the full solution for the mode-mixity angle Ψ with the use of the extended critical buckling stress σ_c^* from eqs. (5) and (6):

$$\tan(\Psi) = \frac{Im(Kh^{i\varepsilon})}{Re(Kh^{i\varepsilon})} = \frac{\cos(\omega^*)+\frac{1}{2}\left(\sqrt{\frac{\sigma}{\sigma_c^*}-1}\right)\sin(\omega^*)}{-\sin(\omega^*)+\frac{1}{2}\left(\sqrt{\frac{\sigma}{\sigma_c^*}-1}\right)\cos(\omega^*)} \quad (7)$$

While the inclusion of real deformation of the buckle through the parameters a_{11}, a_{12} and a_{22} has an impact on the overall results, there is a negligible change in mode-mixity angle Ψ even for $\alpha \to \pm 0.99$ [40].

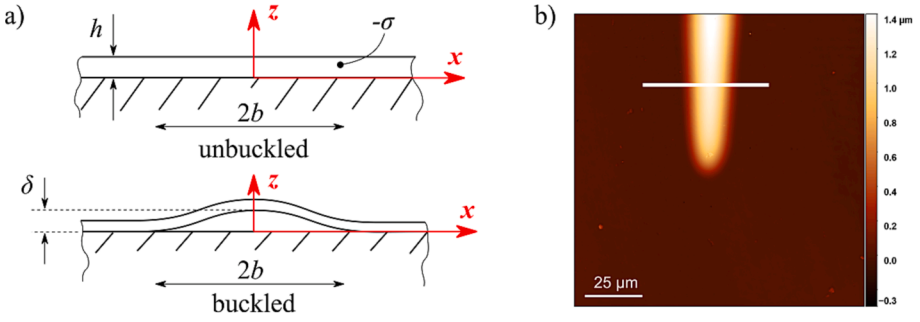

Fig. 1. Thin film buckling delamination: a) geometry of the model of the spontaneous buckling induced by compressive stress in the film with the central coordinate system denoted by red arrows (cross-section) [20]; b) top–view of a typical straight buckle – height profile.

Therefore, when the left side of the eq. (7) does not change, but the extended critical buckling stress σ_c^* is used, the value of the phase factor will be different than for simplified model in eq. (4). Hence, it will be denoted as ω^* for the extended model to avoid confusion in this manuscript.

It should be noted that the full extended model of the buckling delamination has an impact also on the evaluated adhesion energy $\Gamma(\Psi)$ e.g. in eq. (2). However, since the focus of this work is on the mode-mixity, other, non-related changes will not be discussed here.

Assuming the above described model and relation of the buckles to the mode-mixity, the phase factor ω in simplified model and the extended phase factor ω^* (with a_{11}, a_{12} and a_{22}) in the extended model are the only parameters related to the elastic mismatch between the film and substrate materials. The simplified phase factor ω was correlated with the Dundurs parameters (defined in eq. (1)) by Suo and Hutchinson [44] for the parameter α in the range between $\pm$ 0.8 and β in range between $\pm$ 0.4, however, with the use of an iterative method and for a rough resolution of data-points. For use in the H&S model in eq. (4), the phase factor ω was evaluated for a full range of α in two special cases: $\beta = 0$ and $\beta = \alpha/4$, with the statement that for real material combinations "*most of the (α, β) combinations fall between $\beta = 0$ and $\beta = \alpha/4$*" [20]. Moreover, in the section related to a one sided blister, the variation of the phase factor ω for different α and β values is marginalized. Mostly the case of no elastic mismatch, such that $\alpha = \beta = 0$, is investigated more thoroughly, considering the phase factor as a fixed value of 52.1°. Furthermore, forcing the mode-mixity parameter to only be a function of buckle dimensions. Therefore, evaluating the $\Gamma(\Psi)$ via eqs. (2) and (3) does not consider the substrate material. The fact that there is a dependence of the phase factor ω on the material elastic mismatch and the simple relation between the tangent of the mode–mixity angle being the pure ratio of K_{II} and K_I stress intensity factors (4) is true only for $\beta = 0$ has been overlooked by many authors [45–49] ever since.

Additionally, the assumption of real bi-material combinations being in the region between $\beta = 0$ and $\beta = \alpha/4$ in the α-β space does not hold true for modern bi-material systems. As is depicted in Fig. 2, there are numerous material combinations surpassing the $\beta = \alpha/4$ relation, with

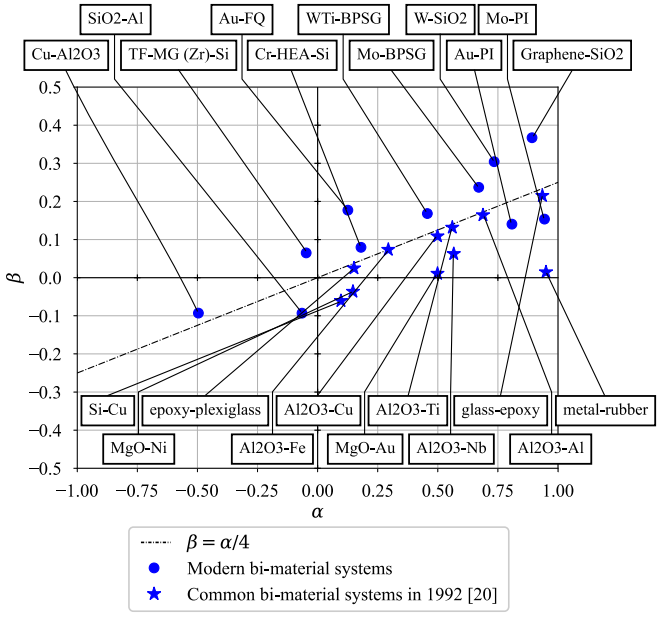

Fig. 2. Comparison between bi-material systems presented in [20] and modern, widely-used bi-material systems depicted in α-β coordinates (filled circle data points, examples taken from various sources [50–58]); BPSG stands for Boro-phosphor-silicate glass, PI stands for polyimide, TF-MG stands for thin film metallic glass, FQ stands for fused quartz and HEA stands for high-entropy alloy.

an extreme case for graphene film on SiO_2 substrate leading to values $\alpha = 0.89$ and $\beta = 0.37$.

For the proper evaluation of the adhesion energy as a function of the mode-mixity angle Ψ and for the description of all possible material combinations the $\omega^*(\alpha, \beta)$ function has to be found, describing the full solution for the buckling delamination. Therefore, the numerical approach to evaluate mode-mixity as a function of Dundurs parameters in a general fashion is presented and compared with the available data.

2. Methods

The main focus of this work is to find a suitable theoretical solution for the mode-mixity angle Ψ and the extended phase factor ω^* as functions of the Dundurs parameters α and β. Therefore, the core methods used were related to theoretical modelling and simulations. However, to demonstrate the influence of the elastic mismatch on the mode-mixity angle Ψ, devised models were applied on an example of real buckling delamination. Hence, presented work contains also an experimental part.

2.1. Numerical model

To properly asses the stress–strain concentration at the front of the delamination crack, a method allowing the calculation of the SIFs has to be used. An original approach by Suo and Hutchinson [44] examined the problem analytically, according to simple Euler's beam theory. Such methodology introduced several implicit simplifications in a form of beam approximation and the use of the small strain theory in terms of continuum mechanics (see e.g. [59]). To avoid the repetition of methodology and to provide more accurate results without the above-mentioned simplifications, the finite element (FE) method was used in terms of this work. All calculations were performed via Python code scripting within the Dassault Systèmes Abaqus 2019 code.

The model retained the geometrical simplification in terms of using 2D plane strain model with the use of one symmetry plane (see Fig. 3), but it allowed the full deformation of both film and substrate, leading to full, extended solution. The main features of the model were set as floating parameters to allow iterative calculations for numerous combinations of the film thickness h, buckle half-width b, residual stress in the film σ, film and substrate Young's moduli E_1 and E_2 and Poisson's ratios ν_1 and ν_2. The model was created as a half-infinite plane in order to avoid shielding effects of the boundaries. The actual delamination allowing to form a buckle was created as a prescribed crack in the film–substrate interface, without modelling any actual delamination process. This approach could be used since dissipation of the energy on thin film delamination does not have any influence on the SIFs at the crack tip in such case, and the only influences are from the geometry of the buckle and material parameters. The symmetrical boundary condition (displacement in the x-direction was fixed to 0) was set in the location of the symmetry plane of the model and the introduction of the compressive stress in the film together with the crack allowed in the model to form the buckle.

Variation of the film and substrate elastic material properties yielded 1129 unique α and β combinations, filling out the full range of possible

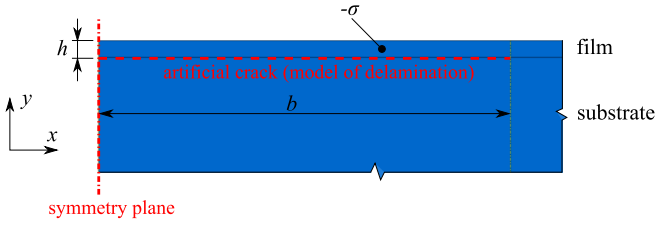

Fig. 3. Geometry model of the film-substrate system for the buckling simulation (unbuckled, initial state).

material combinations (Fig. 4). The dataset included the auxetic materials with the negative Poisson's ratio (for more information, see [60]). Several of the datapoints were calculated more than once with different buckle geometry and/or stress in the film to verify the assumed influence of the geometrical and stress parameters. The model was meshed with linear, plane strain elements (CPE4R, with a hybrid variation CPE4RH for cases with extreme values of used Poisson's ratio, for more information, see [61]). To maintain a reasonable calculation time for high number of model parameters, but with precision accuracy, the optimal mesh size was found, consisting of 25 elements through the film thickness and the element size in the regions of interest (buckled part of the thin film and vicinity of the crack tip) in the direction parallel to the interface and through the substrate thickness was set to increase from 0.05-times the film thickness up to 25-times the film thickness. It was also assumed that the nature of the buckling deformation does not involve any contact stresses causing the interpenetration between the film and substrate in the model. This assumption was checked and confirmed for the modelled geometrical, stress and material parameters used in this study, therefore, no contact elements had to be used, further improving the calculation times.

As results, the geometry of the buckled film (buckle height, w and the lateral deformation of the buckle u) as well as K_I and K_{II} SIFs were used. The SIFs were obtained via the domain integration method [61–63]. The results were subsequently used in evaluation of the phase angle ω and extended phase angle ω^* according to eqs. (3) to (7). The parameters a_{11}, a_{12} and a_{22} were obtained via numerical calculations for each modelled case from the final buckle profile.

2.2. Experiments

Experimental measurements directly used in processing of the presented model to show and prove the impact of the Dundurs parameters and phase angle ω changes are evaluated on the example of four different, 100 nm thin Cu films delaminating from a glass substrate by means of a 500 nm thin stressed Mo overlayer, investigated in a previous work [32]. There, the Cu-glass interface adhesion was investigated as a function of four different Cu microstructures (obtained by using different deposition parameters and annealing treatments) having the same thickness and similar residual stresses that delaminated as straight-sided buckles from a glass substrate using a compressively stressed (-2 GPa), 500 nm thick Mo overlayer. The resulting buckle dimensions (buckle width and height) were then determined using confocal laser scanning microscopy (CLSM) as shown in the height profile of such a buckle in Fig. 1b. Applying the H&S model for straight buckles [20] extended by the delaminating bilayer model proposed by Kriese et al. [66] mixed mode adhesion energies ranging from 2.35 J/m^2 – 4.9 J/m^2 were obtained for the Cu-glass interface, depending on the Cu film microstructure. The experimental setup of the glass-Cu-Mo system is shown in Fig. 5. Hereafter, the experimentally obtained raw data from [32] (previous research of the authors) were used to validate the presented model.

Additionally, the mixed mode adhesion energies $\Gamma(\Psi)$ and mode–mixity angles Ψ for assumed $\omega = 52.1^\circ$ were taken from the original work [32] as well. Evaluation of the real Dundurs parameters was performed with the assumption of equivalent Young's modulus and Poisson's ratio of the Mo-Cu bilayer with a 100 nm thin Cu film and a 500 nm Mo overlayer on top leading to thickness-weighed Young's modulus $E_1 = 285.3$ GPa and Poisson's ratio $\nu_1 = 0.31$. In combination with material properties of the glass substrate ($E_2 = 64$ GPa and $\nu_2 = 0.2$), the resulting elastic mismatch was characterized by the Dundurs parameters $\alpha = 0.65$ and $\beta = 0.26$, showing noticeable mismatch between the elastic parameters of the thin film layer and substrate. In this case, using the thickness-weighed elastic properties of the top bi-layer is a viable simplification since the bi-layer deformation as a whole is the governing factor of the elastic mismatch influence on the mode-mixity.

3. Results

In general, all numerical models have to be verified. In the case of the presented model, the deformed geometry of the buckled film can be compared with experimental data measured on the similar type of buckling delamination. Lassnig et al. [32] performed spontaneous buckling-induced delamination experiments on Mo-Cu-glass system, producing straight and uniform buckles (Fig. 1b). The CLSM measured height profiles of the real buckles can be directly compared to the equivalent FE model, see Fig. 6.

The modelled buckling behaves as expected, the buckle shape corresponds to a typical buckle shape and the stress field around the delamination crack tip exhibit standard mode I + II shape, as depicted in Fig. 6 (for reference see [64]). Furthermore, the direct comparison of the buckle shape between the experimental data and FE simulation in Fig. 7 shows almost identical height profiles. Therefore, the correctness of the FE model has been validated.

Additionally, there is a need to further prove the usability of the FE model SIFs results and the evaluation according to eqs. (3) to (7). Since there is no general way to validate the SIFs results, for this purpose, the $\omega(\alpha, \beta)$ values from the simplified approach were compared with ones presented by H&S [20] for the case of the original spontaneous buckling

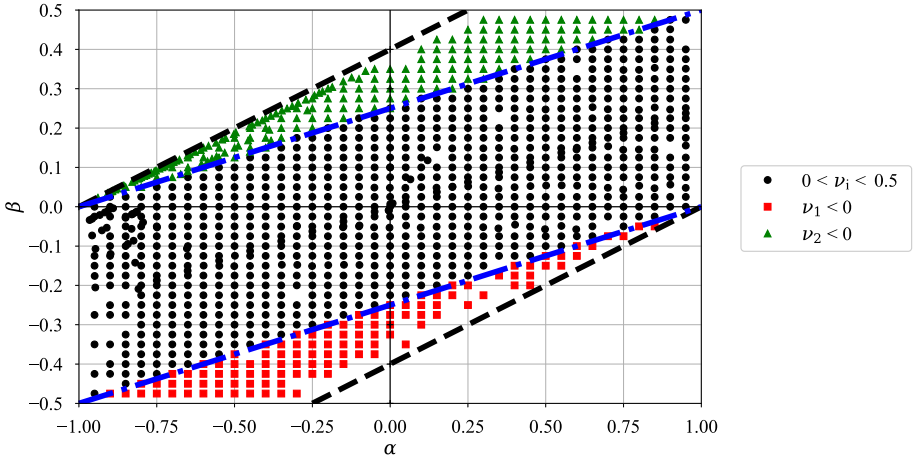

Fig. 4. Modelled combinations of α and β parameters; blacked dashed lines denote the boundaries of the possible (real) material combinations, the blue dash-dotted lines divide the material combinations between materials with negative Poisson's ratio (auxetic materials, see [60]) and "standard" materials with positive Poisson's ratio.

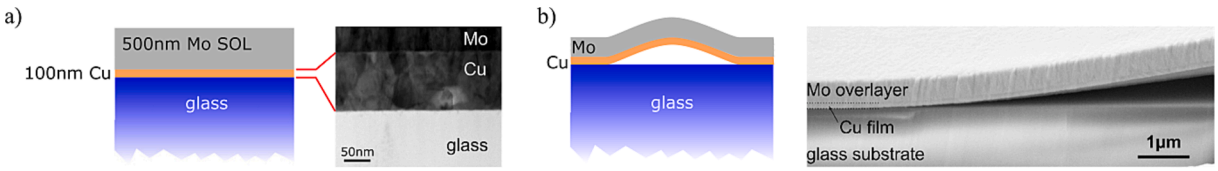

Fig. 5. Visualization of the experiment from [32]: a) scheme and BF-STEM image of the as-deposited bi-layer, b) scheme and FIB cross-sections of the delaminated (buckled) film, showing the onset of the buckle on the FIB cross-section.

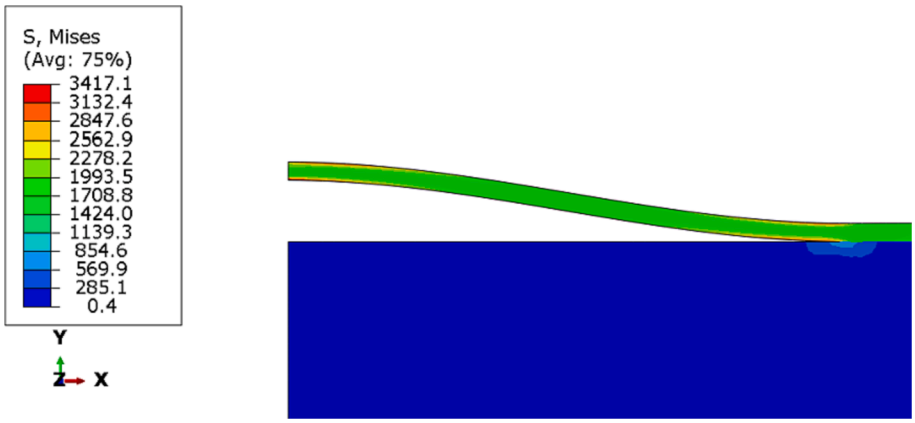

Fig. 6. Deformed buckle from FE model with depicted equivalent (von-Mises) stress contours in MPa.

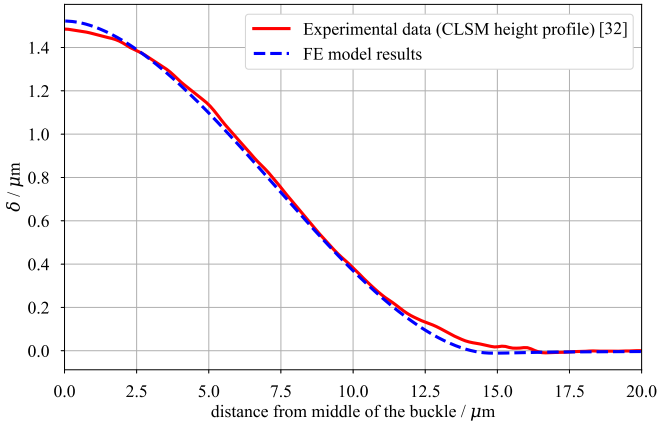

Fig. 7. Comparison of the height profiles of the typical buckle from [32] and the FE model.

delamination. To demonstrate the change in phase factor when the extended solution is used, also the corresponding values of ω^* are plotted alongside the simplified ω.

A direct comparison of the simplified phase factor values ω for $\beta = (0; \alpha/4)$ in Fig. 8 shows a very good agreement between the original and new simplified approach. The slight difference between the numerical and original results for $\alpha > 0.8$ is possibly caused by the more complex nature of the numerical FE model, showing small improvement in regards to original analytical solutions in [20,44]. It can be claimed that the assumption of the elastic beam theory, i.e., cross section perpendicular to the neutral plane, is not violated despite the large deformations considered at the FE calculations. Additionally, when using the extended, more accurate approach, the extended phase factor ω^* shows similar behavior as the original one, however, there is a slight shift towards higher values. This effect is more pronounced for higher α-values, as expected. This difference is caused by the fact, that for the extended model, the elastic mismatch is described not only by the phase factor, but also by the a_{11}, a_{12} and a_{22} parameters evaluated from the real buckle deformation. This shows a necessity of the proper use of the phase factor value depending on the method which is used to assess adhesion alongside its values in full α and β range. This is further demonstrated when all data points (from Fig. 4) of directly evaluated ω and ω^* values were fitted with a surface described by a polynomial function (fifth-degree polynomial in the α direction and third-degree polynomial in β direction) and its resulting contour plot is depicted in Fig. 9.

4. Discussion

While the widely used simplification assuming $\omega = 52.1°$ may be valid for a range of material combinations with use of the simplified model, the newly evaluated numerical results presented in Fig. 9a show that for possible film-substrate material combinations, the simplified phase factor can vary between 30° and almost 80°, which is significantly different than previously assumed value of 52.1°. Moreover, it has to be kept in mind that the simplified approach should be used for material combinations with $\alpha < 0.5$, otherwise, a more general approach with assuming fully deformable model should be used. While it leads to the same mode-mixity values, the extended phase factor ω^* shows deviation from the simplified model in whole α and β spectra (as also seen in Fig. 8). This difference is caused by the fact that the elastic mismatch influences not only the phase factor, but also the value of extended critical stress σ_c^* through the film-substrate deformation. Despite the shift between ω and ω^*, the extended model confirms a strong influence of the Dundurs parameters on the mode-mixity for real–life modern material combinations. This significant deviation is caused solely by the differences in the stress–strain fields within the different materials of the substrate and thin film. While the influence of the elastic mismatch on the mode I loading at the crack tip may be insignificant and the mode I loading is governed mainly by the buckle height and opening, the mode II is largely influenced by the differences in stresses on the film-substrate interface. The mode II governing stress is the shear stress component τ_{12} [64] and because the interface dividing the different materials lies in the mode II deformation plane, it is the most influential mode. Therefore, through the mode II, the elastic mismatch between the film and

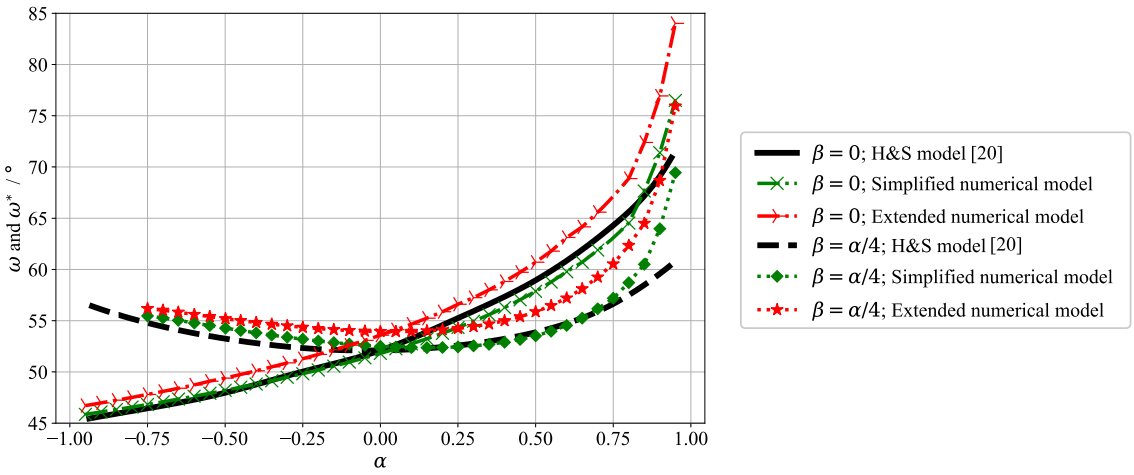

Fig. 8. Comparison of the phase factors ω and ω* for β = (0; α/4) between the new simplified and extended numerical models and original H&S model [20].

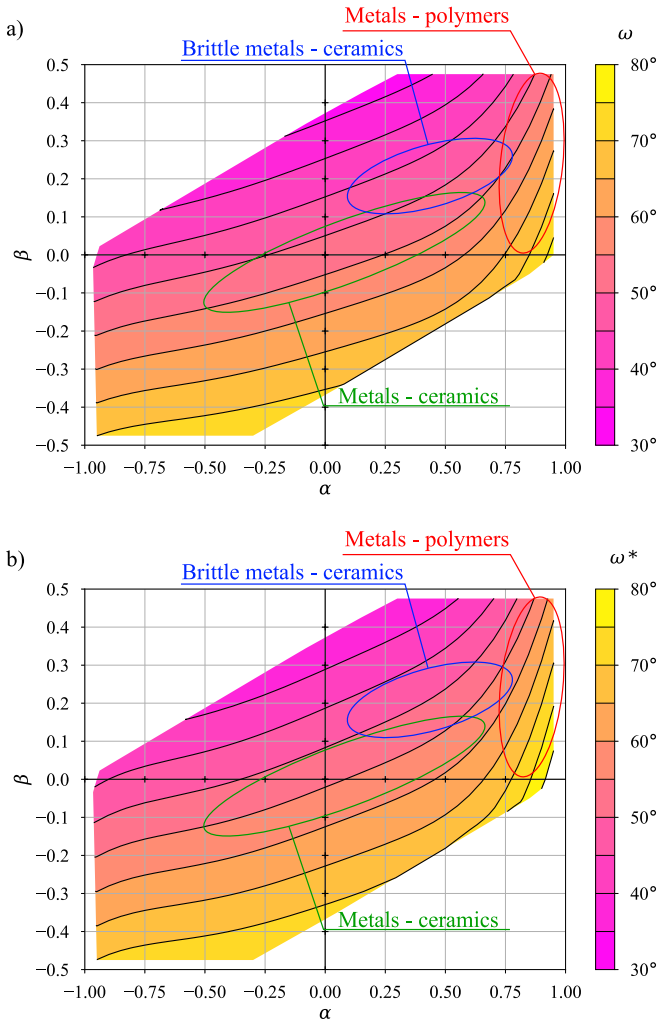

Fig. 9. Plot of the resulting a) simplified phase factor ω and b) extended phase factor ω* obtained from the FE simulations as a function of the α and β parameters; regions of typical α and β combinations (see Fig. 2) are marked in red, blue and green ellipsis; color scale is the same for both cases. A slight shift between ω in a) and ω* in b) towards higher ω*-values as the same color scale is used for both simplified and extended models, similarly to results in Fig. 8, further discussed in Discussion section and Table 1.

substrate causes the change in mode-mixity at the film delamination crack front in the case of the spontaneous buckling.

It can be argued that the extreme ω values are present only in the regions of very rare material combinations. Indeed, it is intuitive that the larger the elastic mismatch, the higher the difference in mode-mixity. This may raise the question, if, despite the large range of ω or ω^*, the assumption that usually used material combinations yield the phase factor close to the case with no elastic mismatch and original idea of $\omega = 52.1^\circ$ (for extended model $\omega^* = 53.99^\circ$) can be still safely used? This can be easily answered by comparing the results in Fig. 9 with the α and β values for modern material combinations depicted in Fig. 2.

The detailed results in Table 1 for real bi-material systems show that according to the presented numerical model (either simplified or extended), several material systems with even higher elastic mismatch show values of ω close to 52.1°. However, there is also an extreme case of the molybdenum thin film on the polyimide substrate (Mo-PI) with a significant elastic mismatch leading to almost 41 % difference when a proper, extended model is used and compared to the value of $\omega^*(0, 0) = 53.99^\circ$. Additionally, five out of eleven examples exhibit the difference between 5 % and 20 %, which can be deemed significant enough to cause unforeseen errors in adhesion energy evaluation.

In order to correctly assess the impact of the presented approach to phase factor, one additional point of view has to be accounted for. The phase factor has a direct impact solely on the mode–mixity angle Ψ and only through it, the ω or ω^* has further implications. According to H&S [20], the mode–mixity angle is constrained in range $\Psi \in \langle -90^\circ; 0^\circ \rangle$ and when the buckle dimensions, σ to σ_c (σ_c^*) ratio and/or phase factor ω (ω^*) leads to angle Ψ outside of the allowed range, it should be assumed $\Psi = -90^\circ$, therefore, pure shear loading is present at the delamination crack front [20,39]. This criterion limits the influence of the elastic mismatch and ω (ω^*) by literally annulling it for $\Psi = -90^\circ$ cases. While the pure mode II loading is a common factor for spontaneous buckling delamination, it is not unusual to experimentally observe spontaneous buckling with Ψ in range between -90° and -67.5°, therefore, putting the phase factor influence back in effect.

Since adhesion energy Γ(Ψ) is a function of the mode-mixity angle, proper evaluation of the mixity angle Ψ is needed for further assessment of the interface fracture criteria. As an example of the influence of the phase factor ω and extended phase factor ω^* on the Γ(Ψ) function, the mode-mixity was evaluated for the case of real buckles on the Mo-Cu-glass system [32] with assumption of original model with $\omega = 52.1^\circ$ (according to $\alpha = \beta = 0$) and according to new numerical results leading to $\omega = 49.95^\circ$ or $\omega^* = 52.98^\circ$ (for $\alpha = 0.65$ and $\beta = 0.26$). While also the values of Γ(Ψ) should be evaluated using the extended model, they are presented only according to calculations with the use of the simplified, original model. The Dundurs parameters of this case are still in a region

Table 1
Modern thin film-substrate material systems as depicted in Fig. 2 with their respective α, β and ω (ω*) values according to presented numerical results in Fig. 9.

Thin film material	Substrate material	α	β	ω / °	Deviation from $\omega = 52.1°$ in %[1]	ω^* / °	Deviation from $\omega^* = 53.99°$ in %[2]
WTi	BPSG	0.46	0.17	49.97	4.10	52.32	3.10
Au	PI	0.81	0.14	61.63	18.29	65.79	21.86
W	SiO_2	0.73	0.30	50.90	2.32	54.48	0.90
Cu	Al_2O_3	−0.50	−0.09	52.50	0.78	53.44	1.02
Graphene	SiO_2	0.89	0.37	56.38	8.21	61.8	14.47
Mo	PI	0.94	0.15	69.77	33.92	75.99	40.75
Mo	BPSG	0.67	0.24	51.69	0.78	54.81	1.52
TF-MG (Zr)	Si	−0.05	0.06	48.78	6.38	50.29	6.86
Au	FQ	0.13	0.18	45.25	13.15	47.12	12.72
SiO_2	Al	−0.07	−0.09	56.37	8.19	57.71	6.90
Cr-HEA	Si	0.18	0.08	50.56	2.95	52.43	2.88

[1] Absolute percent difference in ω according to eq.: $100\% \cdot |\omega - 52.1|/52.1$.
[2] Absolute percent difference in ω^* according to eq.: $100\% \cdot |\omega^* - 53.99|/53.99$.

where the influence of simplifications is small enough [43] and it is less confusing for a pure demonstration of change in mode-mixity.

From Fig. 10, one can clearly see that only a small difference in phase factor (decrease by 2.15° for simplified model and by 0.92° for extended model) shifts the mode-mixity angle Ψ significantly. It should be noted that regardless of the Cu deposition process parameters and subsequent annealing, the film bi-layer material properties did not vary, therefore, all the four subsets have the same values α, β. Presented results show that with a lower value of phase factor, in comparison to the respective value for $\alpha = \beta = 0$, the mode-mixity at the actual delamination crack front shifts to higher shear loading contribution. In the presented case, the shift in mode-mixity angle is approximately 2.5°. While the individual values of Γ(Ψ) are assumed to stay the same, the shift in their position (in regard to the mode-mixity) has a significant impact on the further evaluation of such results. Several semi-empirical functions describing the Γ(Ψ) are widely used to evaluate the pure mode I adhesion energy Γ_I (which can be substituted with $G_{I,c}$) called the practical work of adhesion [65]. This result processing and the Γ_I-value strongly depends on the mode-mixity angles Ψ related to individual measurements. Therefore, to correctly evaluate the Γ(Ψ) as a function for calculating the practical work of adhesion, the mode-mixity dependence on the Dundurs parameters should be used.

It has to be noted that results showed in Fig. 10 do not represent 100 % accurate value for the measured data, due to the use of simplified approach to get the values of Γ(Ψ). Fig. 10 represents only a demonstration of the real impact in changes in the phase factor value. In order to accurately express the Γ(Ψ) function as a whole, more research has to be done.

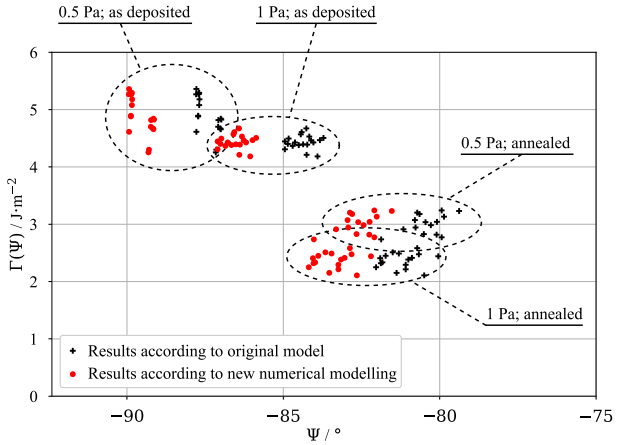

Fig. 10. Comparison of the Γ(Ψ) values with different assumptions for the phase factor obtained from the numerical models for the Mo-Cu-glass system according to [32]; the whole dataset is divided into four groups by the Ar pressure used during the Cu film deposition and subsequent annealing of the samples.

5. Conclusions

Presented numerical approach showed a significant dependence of the crack front mode–mixity on the elastic material properties mismatch in the case of the spontaneous buckling–induced delamination, regardless of what approach is used. The set of widely used modern bi-material systems was shown to reach beyond a three decades old assumption that material combinations fall down between Dundurs parameters values of $\beta = 0$ and $\beta = \alpha/4$. Moreover, the generalized numerical model was used to create an exact expression of the phase factor $\omega(\alpha, \beta)$ and $\omega^*(\alpha, \beta)$ functions. Subsequent comparison of the true ω and ω^* values with the calculations based on assumption of $\omega = 52.1°$ or $\omega^* = 53.99°$ (values for no elastic mismatch) proved the existence of the significant influence of the phase factor and material mismatch on the mode-mixity of the delamination induced by spontaneous buckles.

CRediT authorship contribution statement

S. Zak: Conceptualization, Methodology, Investigation, Formal analysis, Data curation, Writing – original draft, Visualization, Supervision. **A. Lassnig:** Validation, Investigation, Resources, Writing – review & editing. **M. Hrstka:** Software, Validation, Writing – review & editing. **M.J. Cordill:** Validation, Resources, Writing – review & editing.

Declaration of Competing Interest

The authors declare that they have no known competing financial interests or personal relationships that could have appeared to influence the work reported in this paper.

Data availability

Data will be made available on request.

Acknowledgement

Funding of the research has been provided by the Austrian Science Fund FWF within the ESPRIT program (project number ESP 41-N). A. Lassnig acknowledges funding by the FWF under the Hertha Firnberg program (grant number: T891-N36).

References

[1] J. Van Den Brand, M. De Kok, M. Koetse, M. Cauwe, R. Verplancke, F. Bossuyt, M. Jablonski, J. Vanfleteren, Flexible and stretchable electronics for wearable

health devices, Solid. State. Electron. 113 (2015) 116–120, https://doi.org/10.1016/j.sse.2015.05.024.
[2] Y. Yang, W. Gao, Wearable and flexible electronics for continuous molecular monitoring, Chem. Soc. Rev. 48 (2018) 1465–1491, https://doi.org/10.1039/c7cs00730b.
[3] W. Gao, H. Ota, D. Kiriya, K. Takei, A. Javey, Flexible electronics toward wearable sensing, Acc. Chem. Res. 52 (2019) 523–533, https://doi.org/10.1021/acs.accounts.8b00500.
[4] H. Zhang, R. He, Y. Niu, F. Han, J. Li, X. Zhang, F. Xu, Graphene-enabled wearable sensors for healthcare monitoring, Biosens. Bioelectron. 197 (2022), 113777, https://doi.org/10.1016/J.BIOS.2021.113777.
[5] P. Oldroyd, G.G. Malliaras, Achieving long-term stability of thin-film electrodes for neurostimulation, Acta Biomater. 139 (2022) 65–81, https://doi.org/10.1016/J.ACTBIO.2021.05.004.
[6] A. Sharipova, L. Klinger, A. Bisht, B.B. Straumal, E. Rabkin, Solid-state dewetting of thin Au films on oxidized surface of biomedical TiAlV alloy, Acta Mater. 231 (2022), 117919, https://doi.org/10.1016/j.actamat.2022.117919.
[7] G. Mone, The future is flexible displays, Commun. ACM. 56 (2013) 16–17, https://doi.org/10.1145/2461256.2461263.
[8] J. Park, S. Heo, K. Park, M.H. Song, J.-Y. Kim, G. Kyung, R.S. Ruoff, J.-U. Park, F. Bien, Research on flexible display at ulsan national institute of science and technology, Npj Flex. Electron. 1 (2017) 1–12, https://doi.org/10.1038/s41528-017-0006-9.
[9] Y. Li, J.H. Kim, Advances in flexible display materials, SID Symp. Dig. Tech. Pap. 49 (2018) 465–467.
[10] Y. Wang, C. Xu, X. Yu, H. Zhang, M. Han, Multilayer flexible electronics, manufacturing approaches and applications, Mater. Today Phys. (2022), 100647, https://doi.org/10.1016/J.MTPHYS.2022.100647.
[11] Y.Z.N. Htwe, M. Mariatti, Printed Graphene and hybrid conductive inks for flexible, stretchable, and wearable electronics: progress, opportunities, and challenges, J. Sci. Adv. Mater. Devices. (2022), 100435, https://doi.org/10.1016/J.JSAMD.2022.100435.
[12] D.J. Larson, A.K. Petford-Long, Y.Q. Ma, A. Cerezo, Information storage materials: nanoscale characterisation by three-dimensional atom probe analysis, Acta Mater. 52 (2004) 2847–2862, https://doi.org/10.1016/j.actamat.2004.03.015.
[13] R. Ding, S.i. Chen, J. Lv, W. Zhang, X.-D. Zhao, J. Liu, X. Wang, T.-J. Gui, B.-J. Li, Y.-Z. Tang, W.-H. Li, Study on graphene modified organic anti-corrosion coatings: a comprehensive review, J. Alloys Compd. 806 (2019) 611–635.
[14] S.A. Umoren, M.M. Solomon, Protective polymeric films for industrial substrates: A critical review on past and recent applications with conducting polymers and polymer composites/nanocomposites, Prog. Mater. Sci. 104 (2019) 380–450, https://doi.org/10.1016/J.PMATSCI.2019.04.002.
[15] Y. Jin, Z. Chen, W. Yang, X. Yin, Y. Chen, Y. Liu, Electrosynthesis of molybdate-doped P(ANI-co-PY) copolymer coating in ionic liquid for corrosion protection of 304 stainless steel, J. Taiwan Inst. Chem. Eng. 117 (2020) 171–181, https://doi.org/10.1016/J.JTICE.2020.11.027.
[16] J. Bang, S. Coskun, K.R. Pyun, D. Doganay, S. Tunca, S. Koylan, D. Kim, H. E. Unalan, S.H. Ko, Advances in protective layer-coating on metal nanowires with enhanced stability and their applications, Appl. Mater. Today. 22 (2021), 100909, https://doi.org/10.1016/J.APMT.2020.100909.
[17] M. Honarvar Nazari, Y. Zhang, A. Mahmoodi, G. Xu, J. Yu, J. Wu, X. Shi, Nanocomposite organic coatings for corrosion protection of metals: a review of recent advances, Prog. Org. Coatings. 162 (2022), 106573, https://doi.org/10.1016/J.PORGCOAT.2021.106573.
[18] J. Dundurs, Effect of elastic constants on stress in a composite under plane deformation, J. Compos. Mater. 1 (3) (1967) 310–322.
[19] H.G. Beom, Generalized Dundurs Parameters and the Bimaterial Anisotropic Interfacial Crack, in: R.C. Batra (Ed.), Contemp. Res. Eng. Sci., 1995: pp. 66–83. 10.1007/978-3-642-80001-6_5.
[20] J.W. Hutchinson, Z. Suo, Mixed mode cracking in layered materials, Adv. Appl. Mech. 29 (1992) 63–191, https://doi.org/10.1016/S0065-2156(08)70164-9.
[21] M.D. Kriese, W.W. Gerberich, N.R. Moody, Quantitative adhesion measures of multilayer films: Part I. Indentation mechanics, J. Mater. Res. 14 (1999) 3007–3018, https://doi.org/10.1557/jmr.1999.0404.
[22] M. Ortiz, G. Gioia, The morphology buckling-driven thin-film patterns blisters of, J. Mech. Phys. Solids. 42 (1994) 531–559.
[23] E. Barthel, O. Kerjan, P. Nael, N. Nadaud, Asymmetric silver to oxide adhesion in multilayers deposited on glass by sputtering, Thin Solid Films. 473 (2005) 272–277, https://doi.org/10.1016/j.tsf.2004.08.017.
[24] G. Parry, C. Coupeau, J. Colin, A. Cimetière, J. Grilhé, Buckling and post-buckling of stressed straight-sided wrinkles: experimental AFM observations of bubbles formation and finite element simulations, Acta Mater. 52 (2004) 3959–3966, https://doi.org/10.1016/j.actamat.2004.05.011.
[25] M.J. Cordill, N.R. Moody, D.F. Bahr, The effects of plasticity on adhesion of hard films on ductile interlayers, Acta Mater. 53 (2005) 2555–2562, https://doi.org/10.1016/j.actamat.2005.02.013.
[26] J.G. Buijnsters, P. Shankar, W.J.P. Van Enckevort, J.J. Schermer, J.J. Ter Meulen, Adhesion analysis of polycrystalline diamond films on molybdenum by means of scratch, indentation and sand abrasion testing, Thin Solid Films. 474 (2005) 186–196, https://doi.org/10.1016/j.tsf.2004.09.021.
[27] M.J. Cordill, F.D. Fischer, F.G. Rammerstorfer, G. Dehm, Adhesion energies of Cr thin films on polyimide determined from buckling: experiment and model, Acta Mater. 58 (2010) 5520–5531, https://doi.org/10.1016/j.actamat.2010.06.032.
[28] F. Toth, F.G. Rammerstorfer, M.J. Cordill, F.D. Fischer, Detailed modelling of delamination buckling of thin films under global tension, Acta Mater. 61 (2013) 2425–2433, https://doi.org/10.1016/j.actamat.2013.01.014.
[29] V.M. Marx, F. Toth, A. Wiesinger, J. Berger, C. Kirchlechner, M.J. Cordill, F. D. Fischer, F.G. Rammerstorfer, G. Dehm, The influence of a brittle Cr interlayer on the deformation behavior of thin Cu films on flexible substrates: Experiment and model, Acta Mater. 89 (2015) 278–289, https://doi.org/10.1016/j.actamat.2015.01.047.
[30] Q. Zhang, J. Yin, Spontaneous buckling-driven periodic delamination of thin films on soft substrates under large compression, J. Mech. Phys. Solids. 118 (2018) 40–57, https://doi.org/10.1016/j.jmps.2018.05.009.
[31] N. Malkiel, O. Rabinovitch, Dynamic buckling-driven delamination of thin films, Eng. Fract. Mech. 272 (2022), 108691, https://doi.org/10.1016/j.engfracmech.2022.108691.
[32] A. Lassnig, V.L. Terziyska, J. Zálešák, T. Jörg, D.M. Többens, T. Griesser, C. Mitterer, R. Pippan, M.J. Cordill, E. Al., Microstructural Effects on the Interfacial Adhesion of Nanometer-Thick Cu Films on Glass Substrates: Implications for Microelectronic Devices, ACS Appl. Nano Mater. 4 (1) (2021) 61–70. 10.1021/acsanm.0c02182.
[33] L. Euler, Methodus inveniendi lineas curvas maximi minimive proprietate gaudentes sive solutio problematis isoperimetrici latissimo sensu accepti, 1st ed., 1952.
[34] Y.C. Zhou, Z.Y. Yang, X.J. Zheng, Residual stress in PZT thin films prepared by pulsed laser deposition, Surf. Coatings Technol. 162 (2003) 202–211, https://doi.org/10.1016/S0257-8972(02)00581-9.
[35] W.L. Li, W.D. Fei, T. Hanabusa, Effect of deposition condition on residual stress of iron nitride thin films prepared by magnetron sputtering and ion implantation, Appl. Surf. Sci. 252 (2006) 2847–2852, https://doi.org/10.1016/J.APSUSC.2005.04.043.
[36] Q. Xiao, H. He, S. Shao, J. Shao, Z. Fan, Influences of deposition rate and oxygen partial pressure on residual stress and microstructure of YSZ thin films, Thin Solid Films. 517 (2009) 4295–4298, https://doi.org/10.1016/J.TSF.2008.11.138.
[37] A.G. Gómez, A.A.C. Recco, N.B. Lima, L.G. Martinez, A.P. Tschiptschin, R. M. Souza, Residual stresses in titanium nitride thin films obtained with step variation of substrate bias voltage during deposition, Surf. Coatings Technol. 204 (2010) 3228–3233, https://doi.org/10.1016/J.SURFCOAT.2010.03.016.
[38] N. Bradley, J. Hora, C. Hall, D. Evans, P. Murphy, E. Charrault, Influence of post-deposition moisture uptake in polycarbonate on thin film's residual stress short term evolution, Surf. Coatings Technol. 294 (2016) 210–214, https://doi.org/10.1016/J.SURFCOAT.2016.03.092.
[39] M.R. Begley, J.W. Hutchinson, Buckling Delamination, in: Mech. Reliab. Film. Multilayers Coatings, Cambridge University Press, 2017: pp. 137–154. 10.1017/9781316443606.010.
[40] H.H. Yu, J.W. Hutchinson, Influence of substrate compliance on buckling delamination of thin films, Int. J. Fract. 113 (2002) 39–55, https://doi.org/10.1023/A:1013790232359.
[41] H. Mei, Y. Pang, S.H. Im, R. Huang, Fracture, delamination, and buckling of elastic thin films on compliant substrates, in: 2008 11th IEEE Intersoc. Conf. Therm. Thermomechanical Phenom. Electron. Syst. I-THERM, 2008: pp. 762–769. 10.1109/ITHERM.2008.4544345.
[42] B. Cotterell, Z. Chen, Buckling and cracking of thin films on compliant substrates under compression, Int. J. Fract. 104 (2000) 169–179, https://doi.org/10.1023/A:1007628800620.
[43] K. Ustinov, On semi-infinite interface crack in bi-material elastic layer, Eur. J. Mech. A/Solids. 75 (2019) 56–69, https://doi.org/10.1016/j.euromechsol.2019.01.013.
[44] Z. Suo, J.W. Hutchinson, Interface crack between two elastic layers, Int. J. Fract. 43 (1990) 1–18, https://doi.org/10.1007/BF00018123.
[45] M.J. Cordill, D.M. Hallman, N.R. Moody, D.P. Adams, W.W. Gerberich, Thickness effects on the plasticity of gold films, Metall. Mater. Trans. A Phys. Metall. Mater. Sci. 38 A (2007) 2154–2159. 10.1007/s11661-006-9011-7.
[46] M.J. Cordill, D.F. Bahr, N.R. Moody, W.W. Gerberich, Recent developments in thin film adhesion measurement, IEEE Trans. Device Mater. Reliab. 4 (2004) 163–168, https://doi.org/10.1016/j.msea.2006.08.027.
[47] J.-Y. Faou, S. Grachev, E. Barthel, G. Parry, From telephone cords to branched buckles: a phase diagram, Acta Mater. 125 (2017) 524–531, https://doi.org/10.1016/j.actamat.2016.12.025.
[48] A. Bagchi, A.G. Evans, Measurements of the debond energy for thin metallization lines on dielectrics, Thin Solid Films. 286 (1996) 203–212, https://doi.org/10.1016/S0040-6090(96)08551-3.
[49] M.S. Kennedy, N.R. Moody, D.P. Adams, M. Clift, D.F. Bahr, Environmental influence on interface interactions and adhesion of Au/SiO2, Mater. Sci. Eng. A. 493 (2008) 299–304, https://doi.org/10.1016/j.msea.2007.09.081.
[50] A. Lassnig, B. Putz, S. Hirn, D.M. Többens, C. Mitterer, M.J. Cordill, Adhesion evaluation of thin films to dielectrics in multilayer stacks: a comparison of four point bending and stressed overlayer technique, Mater. Des. 200 (2021), 109451.
[51] G.C. Gruber, A. Lassnig, S. Žák, C. Gammer, M.J. Cordill, R. Franz, Synthesis and structure of refractory high entropy alloy thin films based on the MoNbTaW system, Surf. Coatings Technol. 439 (2022) 1–10, https://doi.org/10.1016/j.surfcoat.2022.128446.
[52] C. He, J. Li, X. Wu, P. Chen, J. Zhao, K. Yin, M. Cheng, W. Yang, G. Xie, D. Wang, D. Liu, R. Yang, D. Shi, Z. Li, L. Sun, G. Zhang, Tunable electroluminescence in planar graphene/sio2 memristors, Adv. Mater. 25 (2013) 5593–5598, https://doi.org/10.1002/adma.201302447.
[53] Y. Travaly, L. Zhang, Y. Zhao, R. Pfeffer, K. Uhrich, F. Cosandey, E. Garfunkel, T. E. Madey, Nucleation, growth, and aggregation of gold on polyimide surfaces, J. Mater. Res. 14 (1999) 3673–3683, https://doi.org/10.1557/JMR.1999.0496.
[54] S.J. Lee, T.H. Kim, B.H. Jeong, K.N. Kim, G.Y. Yeom, Properties of tungsten thin film deposited using inductively coupled plasma assisted sputtering for next-

generation interconnect metal, Thin Solid Films. 674 (2019) 64–70, https://doi.org/10.1016/j.tsf.2019.01.051.
[55] A.I. Oliva, R.D. Maldonado, O. Ceh, J.E. Corona, H.G. Riveros, Study of a bimaterial system by an improved dynamical thermal model, Surf. Rev. Lett. 12 (2005) 289–298, https://doi.org/10.1142/S0218625X05007025.
[56] K. Imai, X. Zhou, X. Liu, Application of zr and ti-based bulk metallic glasses for orthopaedic and dental device materials, Metals (Basel). 10 (2020), https://doi.org/10.3390/met10020203.
[57] F. Alves, B. Kearney, D. Grbovic, N.V. Lavrik, G. Karunasiri, Strong terahertz absorption using SiO 2/Al based metamaterial structures, Appl. Phys. Lett. 100 (2012), https://doi.org/10.1063/1.3693407.
[58] S.V. Dmitriev, N. Yoshikawa, M. Kohyama, S. Tanaka, R. Yang, Y. Kagawa, Atomistic structure of the Cu(1 1 1)/α-Al2O3(0 0 0 1) interface in terms of interatomic potentials fitted to ab initio results, Acta Mater. 52 (2004) 1959–1970, https://doi.org/10.1016/j.actamat.2003.12.037.
[59] A.P. Boresi, R.J.J. Schmidt, Advanced mechanics of materials, John Wiley & Sons, New York, 2003.
[60] H. Cho, D. Seo, D.N. Kim, Mechanics of Auxetic Materials, in: Handb. Mech. Mater., Springer, Singapore, 2019: pp. 733–757. 10.1007/978-981-10-6884-3_25.
[61] Dassault-Systemes, Abaqus/CAE 2019 (users manual), (2019).
[62] A.E. Ismail, S. Jamian, K.A. Kamarudin, K.M. Nor, M.N. Ibrahim, M.A. Choiron, An Overview of Fracture Mechanics with ANSYS, Int. J. Integr. Eng. Spec. Issue 2018 Mech. Eng. 10 (2018) 59–67.
[63] M.C. Walters, G.H. Paulino, R.H. Dodds, Interaction integral procedures for 3-D curved cracks including surface tractions, Eng. Fract. Mech. 72 (11) (2005) 1635–1663.
[64] T.L. Anderson, Fracture mechanics: Fundamentals and applications, 2nd ed., CRC Press, Boca Raton (Florida), 1995.
[65] A.A. Volinsky, N.R. Moody, W.W. Gerberich, Interfacial toughness measurements for thin films on substrates, Acta Mater. 50 (2002) 441–466, https://doi.org/10.1016/S1359-6454(01)00354-8.
[66] M.D. Kriese, W.W. Gerberich, N.R. Moody, Quantitative adhesion measures of multilayer films: Part II. Indentation of W/Cu, W/W, Cr/W, J. Mater. Res. 14 (1999) 3019–3026, https://doi.org/10.1557/jmr.1999.0405.